analytical chemistry

Article

pubs.acs.org/ac

3D Droplet Microfluidic Systems for High-Throughput Biological Experimentation

Dong-Ku Kang,[*,†,∥] Xiuqing Gong,[†] Soongwon Cho,[†] Jin-young Kim,[†] Joshua B. Edel,[†] Soo-Ik Chang,[‡] Jaebum Choo,[§] and Andrew J. deMello[*,†,⊥]

[†]Department of Chemistry, Imperial College London, South Kensington, London SW7 2AZ, United Kingdom

[‡]Department of Biochemistry, Chungbuk National University, Cheongjoo 361-763, South Korea

[§]Department of Bionano Technology, Hanyang University, Sa-3-dong 1271, Ansan 426-791, South Korea

Supporting Information

ABSTRACT: Herein, we describe the development of a multilayer droplet microfluidic system for creating concentration gradients and generating microdroplets of varying composition for high-throughput biochemical and cell-based screening applications. The 3D droplet-based microfluidic device consists of multiple PDMS layers, which are used to generate logarithmic concentration gradient reagent profiles. Parallel flow focusing structures are used to form picoliter-sized droplets of defined volumes but of varying composition. As proof of concept, we demonstrate rapid enzymatic activity assays and drug cytotoxicity assays on bacteria. The 3D droplet-based microfluidic platform has the potential to allow for high-efficiency and high-throughput analysis, overcoming the structural limitations of single layer microfluidic systems.

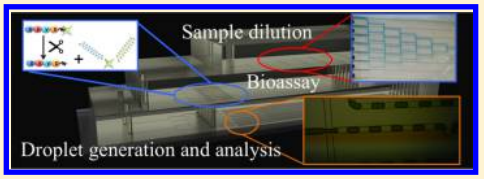

Recent advances in genomics, proteomics, cellomics, and metabolomics have accelerated the creation of libraries of biological and chemical compounds that can modulate various biological processes. Such developments have necessitated the need for high-throughput screening methods where millions of biochemical, genetic, or pharmacological assays can be performed and analyzed in a parallel and rapid fashion to find active compounds against specific biological targets.[1,2] Typically high-throughput screening is performed using high-density microwell plates and robotic dispensing systems.[3] Here, rectangular microwell plates are used to contain reagent volumes ranging from tens of nanoliters to several milliliters of liquid. However, microwell plate based approaches for high-throughput screening are compromised due to the high cost of robotic machinery, evaporation of solvents when sample volumes are reduced, and the need to use relatively large volumes of expensive biological reagents.

Microfluidic systems have recently emerged as a promising experimental platform for performing a diverse range of biological[4−6] and chemical[7,8] experiments in high-throughput manner. Microfluidic-based methods have several advantages when compared to conventional high-throughput screening methods. These include the ability to manipulate and process small assay volumes, minimal consumption of biological reagents, low fabrication costs, reduced analysis times, and the ability to integrate various functional components within a single, monolithic platform.[9]

In particular, droplet based microfluidic systems present a promising opportunity for high-throughput biological analysis.[10−16] In such systems, microdroplets containing nano- to picoliter volumes can be generated at kilohertz frequencies, where each droplet serves as an isolated reaction volume.[17] Since droplet volumes can be reduced down to the femtoliter scale,[18] reactions such as protein−protein interactions[19−21] or DNA hybridization[22] can be performed using billion-fold smaller amounts than conventional biological methods based on 96 microwell plates or enzyme-linked immunosorbent assays (ELISA). Moreover, it should be noted that droplet-based (or segmented flow) microfluidic systems have additional advantages when compared to continuous-flow microfluidic systems such as minimal reagent interaction with channel walls and the absence of residence time distributions. Furthermore, droplet-based microfluidic formats provide for independent control over droplet generation, merging, diluting, splitting, sorting, and analysis on ultrashort time scales.[17,23]

The dilution of one or more reagents is an essential operation in the majority of chemical or biological assays.[7] Surprisingly, the ability to both control and vary the concentration of reagents remains a critical challenge in microfluidic research.[24] In most droplet-based microfluidic systems, concentrations are controlled by varying the volumetric flow rates of reagent streams[20] or by hydrodynamic dispersion prior to droplet formation.[16] However, this approach is usually limited by flow instabilities and restrictive flow rate ranges (approximately 2 orders of magnitude) when using precision syringe pumps.[25] Accordingly, dilution normally requires a series of separate experiments using different substrate concentrations to access concentration ranges typically required for high-throughput screening experiments.

Received: April 19, 2015
Accepted: October 9, 2015
Published: October 9, 2015

DOI: 10.1021/acs.analchem.5b02402
Anal. Chem. 2015, 87, 10770−10778

To address this problem, we recently developed a droplet-based dilution device.[24] Briefly, a concentrated droplet trapped within an asymmetric chamber is exposed to a sequence of smaller buffer droplets within a segmented flow. Through a series of water−oil hydrodynamic interactions, serially diluted droplets of uniform size and spacing could be generated in high-throughput, defining concentration variations in excess of 4 orders of magnitude. More recently, Gielen et al. introduced an open microwell-based gradient concentration droplet generator.[26] Despite its undoubted utility from previous developments, it is difficult to perform and analyze multiple experiments simultaneously using such a component, since the concentration variation is defined by the characteristics of the original trapped droplet, which must be periodically replaced. In addition, Lim and co-workers introduced a parallelized, high-throughput microfluidic emulsifier that can encapsulate nine different substrate concentrations and one reference in parallel for multiplex kinetic assays.[27] Although this device can provide pipet-and-play-based analysis, it lacks control over sample mixing, with all mixing occurring prior to sample addition. For simultaneous analysis of various concentrations, Damean et al. also described a two-layer microfluidic device that contains gradient formation, fluidic mixing, and droplet generation on the bottom layer,[28] with the upper layer containing two chambers that connect to sample inlet/outlet holes for sample injection and effluence. Despite the undoubted utility of such an approach, it is not amenable for complex sample manipulation operations, which are often required for biological experiments such as enzyme inhibitor screening or cell-based biological assays. Since all functional microstructures are located in one fluidic layer (bottom layer) with the other layer only being used to introduce inlet/outlet vias, this type of device could not be used for modular-based devices, where each layer serves specific functions or operations. For example, only two reactant streams are introduced prior to droplet formation, with integration of supplementary channels (to provide additional reagents) before or after droplet formation being difficult, since there are too many microfluidic channels in this fluidic layer. In addition, the formed droplets had to be analyzed within 10 s. Although, sufficient for the stated application, many biological experiments (such as those involving enzymatic reactions and protein interactions) require significantly extended incubation periods.

Recent advances in cellular analysis, genomics, proteomics, and metabolomics, immunoassays, and point of care (POC) diagnostics require multifunctional analytical devices to probe and elucidate biological processes.[29] Droplet-based microfluidics have developed to meet these demands but often rely on the use of single-layered microfluidic devices for a given set of experiments, where each device is used for a specific sample manipulation, such as droplet splitting, merging, trapping, thermal-cycling and sorting.[30−32] To this end, and given the demand for multifunctional droplet-based microfluidic operations, we sought to develop a multilayered, droplet-based microfluidic system by integrating functional microstructures into distinct layers.

Herein, we propose a novel strategy that integrates both concentration gradient generation and parallel droplet generation within a multilayered microfluidic device to generate parallel streams of droplets containing analytes of varying concentration. Specifically, we design a multilayer 3D device that has various functions in each layer such as parallel dilution, sample mixing, droplet generation, and extended time incubation. By adopting a 3D fluidic architecture, it is possible to isolate the droplet generation process from concentration gradient generation, which in turn facilitates the introduction of reagents before and after droplet formation. Using this approach, concentration gradients spanning 2 orders of magnitude can be generated in a direct manner, allowing the efficient screening of enzyme inhibition kinetics and cytotoxicity assays in bacteria.

RESULTS AND DISCUSSION

Gradient Droplet Generation. The generation of concentration gradients relies on appropriately designed networks of microchannels that can generate a range of gradient shapes.[33,34] These systems exploit laminar flows and controlled diffusive mixing of reagents flowing in parallel fluid streams to generate concentration gradients. Linear, logarithmic, and parabolic gradient concentration profiles have all been created by altering channel geometries and concentrations at the inlet channels.[33,35] Recently, Wegrzyn et al. developed a multilayer polycarbonate chip that can generate concentration gradients in a linear profile.[36] Despite its clear utility, the defined approach required complex simulation to generate the desired combination of concentrations. Accordingly, we chose a simple "Christmas tree structure" for our gradient-generating microfluidic network that could be implemented in a single layer and without complex design. Concentration gradients formed in this manner have been shown to be reproducible, stable over time, and do not require active control architectures. A schematic illustration and photographic image of our microfluidic device are shown in Figure 1A and Figure 2A, respectively. A custom built confocal spectrometer was used to analyze fluorescence emission originating from each droplet (Figure 1B). The microfluidic device consists of three PDMS layers. In the top layer, a concentrated sample A is introduced through inlet A and is mixed with dilution buffer (injected through inlet B) to create 8 different concentrations along 8 parallel channels via diffusive mixing (Figure 2B, Supplementary Movies 1 and 2; see blue line). The generated gradient streams are then mixed with an equal volume of sample B (introduced through inlet C) and passed to the bottom layer through the connecting vias (Figure 2C). Water-in-oil droplets with varying compositions of reagent A and fixed concentration of reagent B are then generated by parallel flow focusing structures and mixed using chaotic advection induced by channel winds (Figure 2D, Supplementary Movies 2 and 3). Droplets from each of the flow focusing structures are incubated within long incubation channels (Figure 2E, Supplementary Movie 4). First, droplets containing food dye where generated to assess the uniformity of droplet size between parallel channels (Figure S-1). The deviation in droplet size between parallel channels was calculated to be ±3.87% by analysis of over 28 800 droplets produced by 8 parallel channels (3 600 droplets per each channel).

The dilution capability of the device was subsequently assessed using protein and bacterial cells. First, 1 μM FITC conjugated antibody (anti-CEA monoclonal antibody) was injected through inlet A and mixed with phosphate buffered saline (PBS) solution from inlet B to generate concentration gradient streams. The diluted solutions were then mixed with equal volumes of PBS from inlet C and passed to the bottom layer through interlayer connecting vias. Droplets containing FITC-antibody were generated in the bottom layer using an HFE7500 oil stream containing 2% PFPE−PEG surfactant, and

DOI: 10.1021/acs.analchem.5b02402
Anal. Chem. 2015, 87, 10770−10778

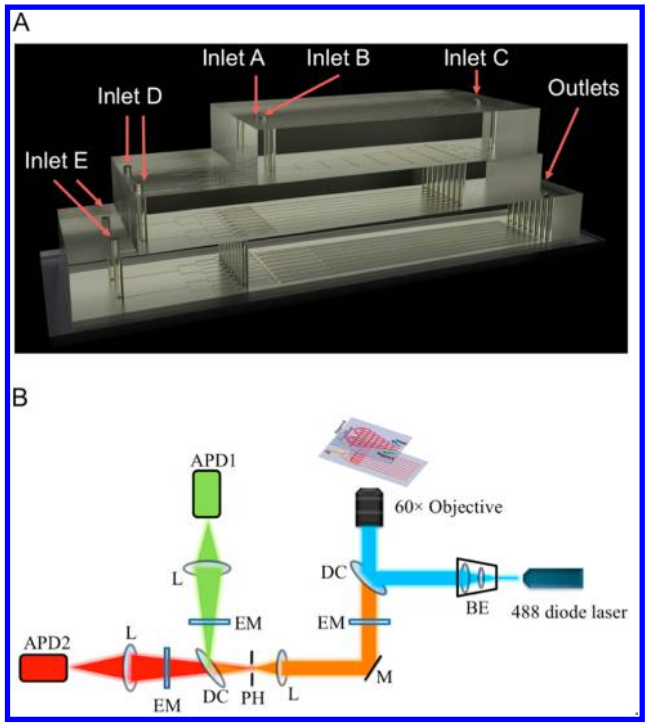

Figure 1. (A) Schematic of the 3D microfluidic device containing 100 μm × 100 μm cross-section channels. Reagents are injected using precision syringe pumps. Reagent A (inlet A) is mixed with water or a buffer solution (inlet B) to generate a concentration gradient. These streams are then mixed with additional samples of fixed volumetric fractions (via inlets C and D). The oil phase is introduced through inlet E to generate a segmented flow. (B) Schematic diagram of the optical detection system used for fluorescence detection. The setup consists of a 488 nm diode laser, two APDs-avalanche photodiode detectors, dc-dichroic mirror, EM-emission filter, PH-pinhole, and L-lens.

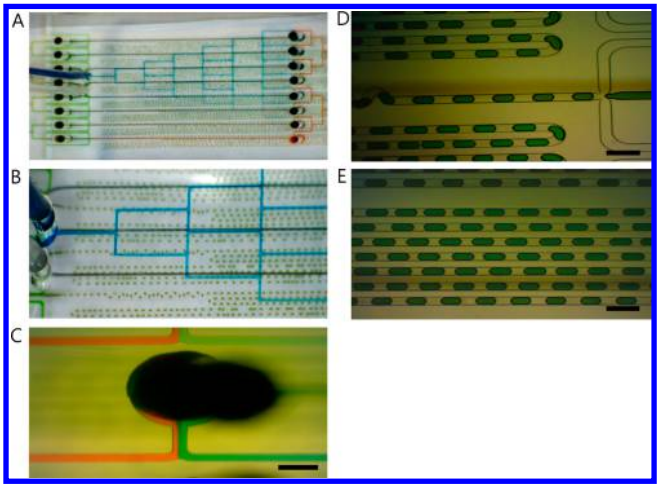

Figure 2. Microfluidic used to assay both enzymatic activity and drug cytotoxicity. (A) Photograph of the microfluidic device. (B) Concentration gradient structure (blue line). (C) Sample mixing junctions and interlayer connection holes between the top and the bottom layers. Scale bar, 200 μm. (D) Parallel flow focusing structures for droplet generation and droplet mixing. Scale bar, 200 μm. (E) Incubation channels. Scale bar, 200 μm.

fluorescence emission originating from each droplet was measured using the custom-built confocal spectrometer. Antibody concentrations were identified from the measured fluorescence intensities (Figure 3A) and compared with theoretical predictions (Figure S-2). Each data point in the

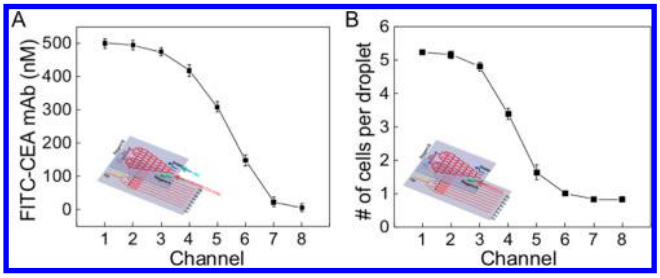

Figure 3. Calibration of concentration gradient generation using FITC-CEA mAb and an *Escherichia coli* suspension after dilution and compartmentalization. (A) 1000 nM FITC-CEA mAb was diluted using PBS within the gradient generation structure and mixed with an equal volumetric proportion of PBS from inlet C to achieve a 2-fold dilution. A concentration gradient of FITC-CEA mAB (500 nM to 0 nM) was created in the top layer and green fluorescence detected from droplets. The concentration of each droplet was then calculated from this measurement. Each data point is the average of ~3 600 droplets. Data are represented as mean ± s.d., n = 3. (B) Distribution of bacterial cells in droplets after dilution. SYTO 9 stained bacterial cells were injected and diluted in the top layer and fluorescence traces used to identify *E. coli* cells within droplets. The average number of cells per droplet was extracted. Each data point is the average of ~3 600 droplets and data are represented as mean ± s.d., n = 3.

microfluidic assay represents an average of 10 800 measurements. A characteristic sigmoidal decrease in concentration was obtained over the range from 500 nM to 5.6 nM using FITC-antibody, which is in excellent agreement with theoretical predictions (see Figure S-2B). Using this approach, concentration gradients spanning 2 orders of magnitude can be generated in a direct manner continuously, allowing the high-throughput biological experiments.

The ability to dilute particle-laden streams was also tested with bacterial cells. A SYTO 9 stained *Escherichia coli* (*E. coli*) suspension in LB (Luria−Bertani) broth, was diluted with LB broth and generated concentration gradient streams were encapsulated in microdroplets. SYTO 9, a DNA intercalating dye is cell membrane permeable and has an emission maximum of 498 nm and an excitation maximum of 482 nm. LB medium also provides a weak fluorescence background that is useful in defining aqueous droplet boundaries. Photon bursts, corresponding to the presence of individual cells, were distinguished from the background droplet signals by post acquisition data analysis.[37] The full width half-maximum (fwhm) of fluorescent bursts arising from *E. coli* cells were calculated to be 30 times shorter than the background droplet events, which is consistent with the relative length of droplets (50 μm) and *E. coli* cells (1.5−2 μm) (Figure S-3A). Figure 3B illustrates average cell occupancies for each of the parallel droplet generation channels. The distribution of cell occupancy within individual droplets for each microfluidic channels is described in Figure S-3B. The characteristic sigmoidal decrease in the average cell occupancy was observed over all channels. These experimental measurements are in excellent agreement with the theoretical predictions (Figure 3B and Figure S-2) and demonstrate the operational functionality of the device for concentration dilution followed by droplet generation.

We found that the gradient concentration between successive channels resembles a sigmoidal function, with changes in concentration being small for the first and last channels and

DOI: 10.1021/acs.analchem.5b02402
Anal. Chem. 2015, 87, 10770−10778

large for channels located in the middle of the device. However, linear gradient concentration profiles can be created and concentration differences adjusted by altering channel geometries and concentrations at the inlet channels when required.[34]

Enzyme Kinetics and Inhibition Assays. To demonstrate the potential of our approach for drug screening, the enzymatic activity of caspase-3 and the inhibitory effects of AC-DEVD-CHO (Ac-Asp-Glu-Val-Asp-CHO) on caspase-3 activity were measured using a fluorescence-based detection system. The analysis of disease related enzymatic activities is recognized to be one of the most important factors in diagnostics[38,39] and early stage drug screening processes,[40,41] and indeed various neuronal diseases, autoimmune diseases and cancers have been related to enzyme deficiency or overproduction.[42−45] More specifically, it has recently been reported that an increase in caspase activity triggers early synaptic dysfunction in Alzheimer's disease[42] and that excessive caspase activities are also associated with Hodgkin's[43,44] and Parkinson's disease.[45] Conversely, a deficiency in active caspase has been observed for various cancers, autoimmune diseases, and neurodegenerative disorders.[46−50] Unsurprisingly, over recent years, there have been many attempts to develop inhibitors and activators for caspase. Accordingly, caspase-3, the most important caspase among the caspase family,[42,51] was chosen as a model system for demonstrating the use of 3D microfluidic systems for high-throughput screening applications.

Figure 4A illustrates the fluidic scheme adopted. By using Rh110 conjugated DEVD (Ac-DEVD-rh110) as a substrate against active caspase-3, we were able to monitor enzymatic activity. Caspase-3 activity was measured dose dependently as a function of substrate concentration. Concentration gradients of Ac-DEVD-rh110 were created, mixed with fixed concentrations of caspase-3, and compartmentalized within droplets. Caspase-3 concentrations of 0, 5, 7.5, and 10 μM were used for all experiments. Cleavage of Ac-DEVD-Rh110 by caspase-3 releases the Rh110 fluorophore which exhibits a bright green fluorescence[52] (Figure 4B). Figure 4C shows the kinetic data from the enzymatic reaction between caspase-3 and Ac-DEVD-Rh110. Curves were constructed using the fluorescence intensities of droplets in each of the 8 parallel channels with flow rates of $V_{\text{inlet A (200 }\mu\text{M Ac-DEVD-rh110)}} = V_{\text{inletB (assay buffer, pH 7.4)}} = 0.25\ \mu\text{L min}^{-1}$, $V_{\text{inlet C (Caspase-3)}} = 0.5\ \mu\text{L min}^{-1}$, and $V_{\text{inlet D (oil)}} = 2\ \mu\text{L min}^{-1}$. Enzyme kinetics were analyzed by the Michaelis−Menten equation, i.e.,

$$V_o = \frac{V_{max}[S]}{K_M + [S]} \quad (1)$$

Here V_o is the rate of conversion, V_{max} is the maximum rate of conversion, [S] is the substrate concentration, and K_M is the Michaelis constant. The Michaelis constant defines the substrate concentration at which the rate of conversion is half of V_{max} and approximates the affinity of the enzyme for the substrate. The experimental K_M values for the enzymatic activity of caspase-3 toward Ac-DEVD-Rh110 were calculated to be 3.98 ± 0.60 μM and 19.06 ± 3.33 μM for our microfluidic device and 96 well plate based measurements, respectively (Figure S-4A). Both values compare well with the value of 6.25 μM reported in the literature.[53] To examine the inhibitory effects of Ac-DEVD-CHO and mixtures of random peptide sequences containing 6 amino acids on the caspase-3 activity, a three layered microfluidic chip was designed and fabricated

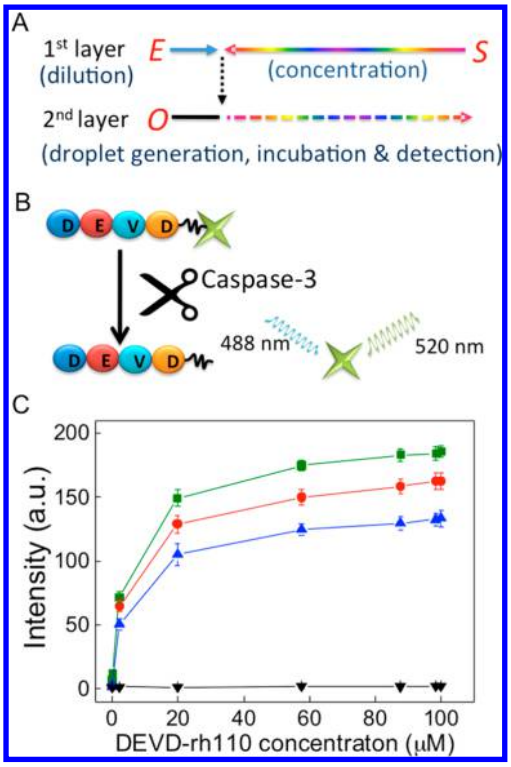

Figure 4. Application of the microfluidic platform in the enzymatic assay of caspase-3. (A) Schematic of the droplet dilution and reaction process. Two layered microfluidic devices were used for the enzymatic assay. Substrate (S) was injected through inlet A to generate a concentration gradient and mixed with enzyme (E) in the first layer and oil (O) in the second layer to generate droplets. (B) Enzymatic reaction between active caspase-3 and DEVD-Rh110. (C) Experimental kinetic data from the enzymatic reaction between caspase-3 and DEVD-Rh110. Initial DEVD-Rh110 concentration was 100 μM and caspase-3 concentrations were 0 μM (aqua ▼), 5 μM (blue ▲), 7.5 μM (red ●), and 10 μM (■). Each error bar represents the standard deviation extracted from 100 measurements. Each data point is the average of ∼3 600 droplets. Data are represented as mean ± s.d., n = 3.

according to the scheme shown in Figure 5A. Caspase-3 was mixed with diluted Ac-DEVD-CHO or a random peptide mixture in the first layer. Each mixture was then combined with Ac-DEVD-Rh110 in the middle layer. In the third layer, droplets containing 50 μM of Ac-DEVD-Rh110, 10 nM of caspase-3, and different concentrations of the inhibitors were generated from each channel. As shown in Figure 5B, the activity of caspase-3 was inhibited by Ac-DEVD-CHO in a dose-dependent manner. At 50 nM, Ac-DEVD-CHO caused the inhibition of more than 85% of the caspase-3 activity in the control experiment. Indeed, the IC_{50} value was calculated to be 5.76 ± 0.42 nM which is in excellent agreement with the literature value of 4.19 nM.[54] A similar IC_{50} value of 1.13 ± 0.17 nM was also obtained by 96 well plate based measurements (Figure S-4B).

Drug Susceptibility Testing. The effects of a drug on an organism are complex and involve multiple networks between biomolecules that cannot be predicted using biochemical assays.[55] This complexity has led to a pressing need for cell-based screening methods able to predict organism response. To validate the potential use of our microfluidic platform for drug susceptibility testing and cell based drug screening, the effects

DOI: 10.1021/acs.analchem.5b02402
Anal. Chem. 2015, 87, 10770−10778

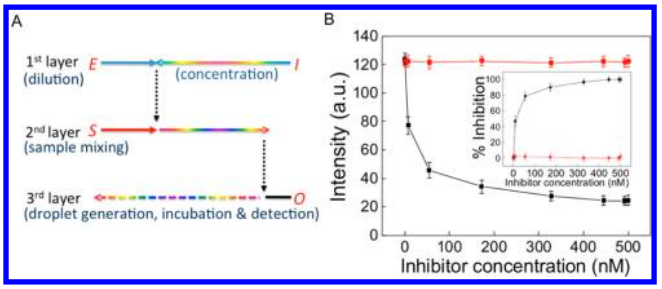

Figure 5. Application of the microfluidic platform for inhibition assay. (A) Schematic of the dilution and reaction processes. Inhibitor (I) and enzyme (E) were injected in the first layer and substrate (S) injected in the second layer. The mixed streams were passed into the third layer and droplets generated by the oil phase (O). (B). The inhibitory effects of DEVD-CHO (■) and random peptides (red ●) on caspase-3 activity. Each error bar represents the standard deviation extracted from 100 measurements. Inset: The percentage inhibition of DEVD-CHO (■) and random peptides (red ●) on caspase-3 activity. Each data point is the average of ∼3 600 droplets and data are represented as mean ± s.d., n = 3.

of antibiotics on bacterial cells were investigated using a fluorescent viability assay.

First, *E. coli* cells were either killed by treatment with 100% methanol or maintained as a healthy *E. coli* cell population. Live and dead cells were then injected into inlet A and inlet B (Figure 1A), respectively, and mixed in the gradient generation structure to yield parallel channels containing different proportions of live and dead cells. Cell mixtures were fluorescently stained using 1 μM SYTO 9 and 1 μM propidium iodide (PI) and then encapsulated within droplets in the bottom layer as previously described. After droplet generation, green (520 nm) and red fluorescence (620 nm) were detected from each of the 8 channels and analyzed to assess viability. The membrane permeable SYTO 9 stains both live and dead cells while PI stains only dead cells whose membrane has been compromised (Figure S-5). SYTO 9 has an excitation maximum of 482 nm and an emission maximum of 500 nm, while PI has an excitation maximum of 528 nm and an emission maximum of 617 nm. This means that dead cells will exhibit both green and red fluorescence emission, while live cells will only fluoresce in the green. Representative fluorescence traces of dead and live cells are shown in Figure 6A. The droplet boundaries are highlighted by dotted lines and the fluorescence originating from contained cells indicated using triangular markers for both red and green traces (Figure 6B). It can be seen that the dead cell percentage decreases from 100% in channel 1 to 20% in channel 8 with the expected sigmoidal pattern (Figure 6C). The deviations of dead cell percentages in channels 6, 7, and 8 from the theoretical expectation are almost certainly due to a 10−20% reduction in cell viability during cell encapsulation, a feature observed previously.[32] A cell death rate of 20% was consistently observed and deemed inherent to the microfluidic system. This places a lower limit on cytotoxicity assays, as described previously.[32] We hypothesize that such cell death is due to shear forces on the cells during encapsulation or centrifugal forces within the syringe caused by the magnetic stirrer bar used to prevent precipitation of the *E. coli* cells.

To quantitatively analyze the effects of antibiotics, both ampicillin sensitive and resistant *E. coli* cells were employed. A solution containing 100 μg/mL ampicillin was introduced into the microfluidic device and diluted using the gradient generator. The diluted ampicillin solution was then mixed with either ampicillin-sensitive cells or ampicillin-resistant cells and passed down to the bottom layer for droplet generation. Droplets containing *E. coli* cells and varying concentrations of ampicillin were collected into syringes connected to each outlets for incubation over a period of 4 h. Collected droplets were then reinjected into a secondary microfluidic device containing flow-focusing oil stream to space droplets for analysis. The final

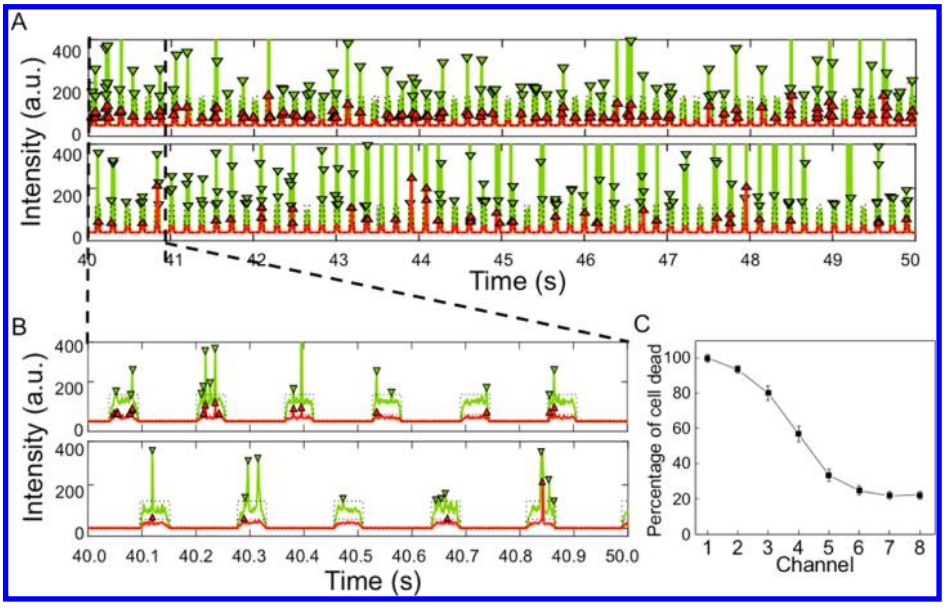

Figure 6. Viability assay performance. (A) Representative fluorescence burst scan of dead (top) and live (bottom) *E. coli* cells recorded over a period of 10 s. The fluorescence signature of a droplet was characterized by a homogeneous rectangular cross section. Spiked peaks on top of this signature signify the presence of cells and are indicated by the triangular markers. (B) Dead cells (top) exhibit both green and red fluorescence and live cells (bottom) only show green fluorescence. Coincident events from both green and red channels correspond to dead cells. (C) Live and dead cells were mixed in different proportions using the gradient dilution chip and the fluorescence traces measured in each channel. Each data point is the average of ∼3 600 droplets and data are represented as mean ± s.d., n = 3.

DOI: 10.1021/acs.analchem.5b02402
Anal. Chem. 2015, 87, 10770−10778

concentrations of antibiotic within each droplet population were varied as 0, 0.78, 5.47, 17.19, 32.81, 44.53, 49.21, and 50 μg/mL respectively over each of the eight channels. It was observed that the proportion of dead cells increased in a dose dependent manner for ampicillin-sensitive cells, with 80% dead cells being observed at an ampicillin concentration of 30 μg/mL. Conversely, we observed no ampicillin-induced cell death for ampicillin-resistant cells (Figure 7B) accounting for the 20% loss of cell viability during the cell encapsulation process for both antibiotic sensitive and resistant cells.

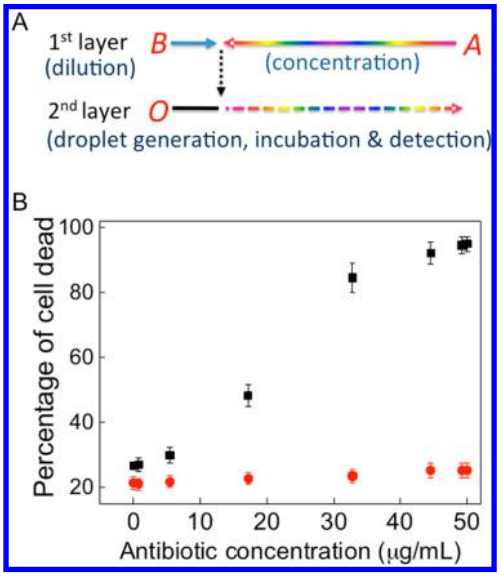

Figure 7. Effects of antibiotics on the viability of the bacterial cells. (A) Schematic of a two-layered microfluidic chip for cell viability measurements. Bacterial cells and ampicillin were injected in the first layer and then passed into the second layer to generate droplets containing fixed cell density and varying concentrations of antibiotics. (B) The effects of antibiotics on antibiotic-resistant (red ●) and antibiotic-sensitive bacterial cells (■). Encapsulation of the bacterial cells and antibiotics within each droplet is followed by incubation for 4 h. Each data point is the average of ∼3 600 droplets and data are represented as mean ± s.d., n = 3.

In summary, we have demonstrated a novel platform for the high-throughput dilution, compartmentalization, and simultaneous monitoring of parallel experiments. Compared to conventional single layered microfluidic systems, our approach provides for significant operational flexibility when generating parallel streams of droplets for high-throughput screens. The entire screening process is shown to remain stable over long periods of time, with devices being easy to handle and fabricate. We note that greater concentration variation ranges can be accessed through parallelization of the basic device architecture and more complex concentration gradient profiles can be created through adoption of different channel geometries. Furthermore, it is important to mention that issues related to precise layer alignment can be addressed through the use of automated-[56] or semiautomated[57] layer-aligning methods. It is also expected that such 3D structured microfluidic devices have the potential to provide a novel and practical platform for performing high-throughput experimentation at low unit cost. Moreover, the development of 3D-printing technologies will allow us to integrate complex functions into the microfluidic system such as those described by Bhargava and co-workers, who recently introduced a modular 3D microfluidic device for 3D mixing, droplet generation, and detection.[58]

MATERIALS AND METHODS

Microfludic Device Fabrication. A schematic of the fluidic chip design and operating mechanism is shown in Figure 1A. The fluidic channel and pillars were fabricated in polydimethylsiloxane (PDMS) using standard soft lithographic techniques.[59] Briefly, PDMS base and curing agent (Sylgard 184; Dow Corning, Wiesbaden, Germany) were mixed in a ratio of 10:1 w/w, degassed, decanted onto a SU8-on-Silicon wafer master (IDB Technologies Ltd., Wiltshire, U.K.), and cured overnight in an oven at 65 °C. After curing, the structured PDMS layer was removed from the master, with the inlet, interlayer connecting and outlet holes being formed using a 1 mm punch (BIOPSY punch, Kay Industries Co., Gifu, Japan). Three PDMS layers were designed and fabricated in this manner. The PDMS layers were initially treated with an oxygen plasma before they were aligned to each other under a stereomicroscope by matching inlet and outlet vias. The *top* layer comprised a dilution structure for reagent A and junctions for the mixing of diluted reagent A and reagent B. The *bottom* layer comprised droplet generation modules and the *middle* PDMS layer contained additional sample injectors used in some experiments. The PDMS layers and 1 mm microscope slide glass substrates were bonded immediately after exposure to an oxygen plasma (Harrick Plasma Cleaner RD-002)

Fluid Components. For the characterization of dilution capacity, deionized (DI) water containing food dye (Black, Kraft Foods, Northfield, IL) and PBS (137 mM NaCl, 2.7 mM KCl, 10 mM Na_2HPO_4, 2 mM KH_2PO_4, pH7.4) were used as the aqueous phase. HFE-7500 fluorocarbon oil (Dow Corning, Midland, MI) containing 2% (w/w) PFPE−PEG (perfluorinated polyethers with polyethylene glycol) surfactant was used as the oil phase. The biocompatible fluorinated surfactant was synthesized according to the method described by Chen et al.[60] Krytox 157FS(H) (100 g, MW ∼5000 g/mol, Dupont, U.K.) was dissolved in 100 mL of anhydrous HFE-7100 (Sigma-Aldrich, U.K.) and mixed with excess oxalyl chloride (25 g, Sigma-Aldrich, U.K.). The reaction mixture was then left stirring overnight at 85 °C under an argon atmosphere. A light yellow product was obtained after solvent removal by rotary evaporation and high vacuum. This product was mixed with Jeffamine XTJ 501 (6.93 g, MW 900 g/mol, Sigma-Aldrich, U.K.) and dissolved in a solvent mixture consisting of HFE 7100 (100 mL) and anhydrous dichloromethane (100 mL, Sigma-Aldrich, U.K.). The reaction mixture was heated to 65 °C and stirred for 2 days under an argon atmosphere, resulting in a milky white product. After solvent removal by rotary evaporation, the product was centrifuged at 8000 rpm for ∼10 min to remove the white residue. The product then was dried in a vacuum desiccator for 24 h and used without further purification.

High-Througput Detection and Data Analysis. Microfluidic devices were placed on a motorized stage and appropriately aligned with a custom-built confocal spectrometer[61] (Figure 1B). The spectrometer consisted of a 488 nm CW air-cooled argon ion laser excitation source. A dichroic mirror (505DRLP02; Omega Optical, Brattleboro, VT) was used to reflect the 488 nm radiation and so define a vertical axis, normal to the surface of the optical table. A 40× microscope objective was employed to bring the light to a tight focus within the microfluidic channel. Subsequently, fluores-

DOI: 10.1021/acs.analchem.5b02402
Anal. Chem. 2015, 87, 10770−10778

cence emission was collected with the same high-NA objective and transmitted through the same dichroic mirror. An emission filter (515EFLP; Omega Optical) removed any residual excitation light. The fluorescence is then spectrally separated by another dichroic mirror (z630rdc, Chroma Technology Corp.). In the first channel (green detector), fluorescence reflected by the dichroic mirror is further filtered by an emission filter (hq540/40m, Chroma Technology Corp.) and focused by a plano-convex lens (f = 25.4 mm, Thorlabs, Ltd., U.K.) onto an avalanche photodiode (SPCM-AQR-141, EG&G Canada, Vaudreuil, Quebec, Canada). In the second channel (red detector), fluorescence passed through the dichroic mirror and is filtered by another emission filter (hq640lp, Chroma Technology Corp.) and focused by a plano-covex lens (f = 25.4 mm, Thorlabs, Ltd., U.K.) onto a second avalanche photodiode (SPCM-AQ-13, PerkinElmer, Canada). The APD detectors operating in single-photon counting mode convert single photon events into TTL pulses (1 photon equals 300 ps 5 V pulse). A digital counter (PCI 6601, National Instruments, U.K.) in combination with a program written in LabView is used to control and perform data acquisition.

For all assays described herein, the droplet generation frequency was maintained at approximately 50 Hz to ensure adequate sensitivity when monitoring single bacteria. Typically, droplet streams were analyzed over a period of 60 s from each channel (and repeated 10 times). This equates to a total time of 600 s and 3 600 droplets. In total 28 800 droplets were analyzed for each set of experiments (i.e., 3 600 droplets in 8 channels), with all experiments being repeated three times.

Enzyme Assay. Caspase-3 (abCAM, Cambridge, U.K.) and its substrate Ac-DEVD-rh110 (AnaSpec, Fremont) were used for enzyme activity measurements. Ac-DEVD-rh110 (200 μM) was injected to inlet A and diluted with an assay buffer (100 mM NaCl, 50 mM HEPES, 10 mM DTT, 1 mM EDTA, 10% glycerol, pH 7.4), which was injected to the inlet B. The 5, 7.5, and 10 μM caspase 3 was injected through inlet C and combined with diluted Ac-DEVD-Rh110 solutions. Droplets were incubated for 10 min in the device, and "green" fluorescence from the enzymatic reaction was detected using the custom-built confocal spectrometer. To demonstrate the competitive inhibition effect of an inhibitor, Ac-DEVD-CHO (AnaSpec, Fremont, CA) was used as an antagonist against Ac-DEVD-Rh110 to disturb the enzymatic reaction between caspase-3 and Ac-DEVD-Rh110. The 1000 nM Ac-DEVD-CHO was injected to inlet A and diluted with assay buffer from inlet B. Diluted streams of Ac-DEVD-CHO were mixed at the junction with 10 nM caspase 3 on the top layer and passed down to the middle layer to combine with a 50 μM Ac-DEVD-Rh110 stream and then to the bottom layer to generate picoliter-volume droplets. Generated droplets were incubated for 10 min and "green" fluorescence detected using the confocal spectrometer. All data were collected over a period of 600 s and all experiments were replicated three times with triplicate repeated measures within each replication.

Cell Viability Assay and Drug Susceptibility Testing. Bacterial cells were killed by treatment with 100% methanol for 1 min and then centrifuged to remove supernatant. Cell pellets were washed three times with PBS, and it was then resuspended in LB broth. Both live and dead cell suspensions were injected into inlet A and inlet B, respectively, mixed in the gradient generation structure (Figure 1A), and stained with 1 μM SYTO 9 (Invitrogen, Carlsbad, CA) and 1 μM PI (Invitrogen, Carlsbad, CA) introduced through inlet C. After droplet generation, "green" (520 nm) and "red" (620 nm) fluorescence emission were detected from each of the eight channels using the custom-built confocal spectrometer and analyzed using Matlab R2009b to quantify the viability of the cells.

For the drug susceptibility testing, a 100 μg/mL ampicillin solution (dissolved in PBS) and a PBS solution were injected into inlet A and inlet B, respectively, and mixed in the gradient generation structure (Figure 1A). Ampicillin-resistant *E. coli* TOP10 cells or ampicillin-sensitive *E. coli* BL21 cells were also introduced through inlet C and mixed with various concentrations of ampicillin from the dilution structure in the top-layer. The mixtures of bacterial cells and antibiotics were transferred to the bottom layer and then mixed with 1 μM SYTO 9 and 1 μM propidium iodide (PI) injected through the second layer (inlet D) (Figure 1A). After droplet generation on the third layer, droplets were collected in the syringes and also incubated for 4 h at room temperature. To assess cell viability in droplets, collected droplets were then reinjected into the microfluidic device incorporating a flow focusing oil stream to space droplets. All data were collected over a period of 600 s and all experiments were replicated three times with triplicate repeated measures within each replication. Thresholding was used to reduce the false positives when determining red and green peaks from the droplets. A photon counting histogram was used as the starting point for determining an appropriate threshold for a given data set as previously described.[37] Since the background shot noise exhibits Poissonian statistics,[62] the early part of the PCH dominated by low, background counts is modeled to a Poisson distribution, which then sets a statistical limit for the droplet threshold. Photon counting events above this threshold were identified as droplets. By analogy with Gaussian systems, the selected peak discrimination threshold can be defined as three standard deviations from the mean count background rate.

■ ASSOCIATED CONTENT

Supporting Information

The Supporting Information is available free of charge on the ACS Publications website at DOI: 10.1021/acs.analchem.5b02402.

Droplet size analysis, theoretical concentration gradient in the device, quantification of the number of cells per droplet, reaction curves, and confocal fluorescence images (PDF)

Video demonstrating 3D droplet-based microfluidic device (AVI)

Video demonstrating that gradient generation, sample mixing and droplet generation in two layered 3D droplet-based microfluidic device (AVI)

Video demonstrating reagent introduction through the middle layer and subsequent droplet generation in the bottom layer (AVI)

Droplet incubation in the bottom layer (AVI)

■ AUTHOR INFORMATION

Corresponding Authors

*E-mail: kangdk@uci.edu.

*E-mail: andrew.demello@chem.ethz.ch.

Present Addresses

[‖]D.-K.K.: Department of Pharmaceutical Sciences, Department of Biomedical Engineering, University of California Irvine, CA, 92697.

DOI: 10.1021/acs.analchem.5b02402
Anal. Chem. 2015, 87, 10770−10778

[⊥]A.J.d.M.: Department of Chemistry and Applied Biosciences, Institute for Chemical and Bioengineering, ETH Zurich, Vladimir-Prelog-Weg 1, Zurich, 8093, Switzerland.

Author Contributions

The manuscript was written through contributions of all authors. All authors have given approval to the final version of the manuscript

Notes

The authors declare no competing financial interest.

■ ACKNOWLEDGMENTS

This work was supported by Newton International Research Fellowship from Royal Society UK and the Global Research Laboratory Program of the National Research Foundation of Korea (Grant Number K20904000004-11A0500-00410). We thank Mr. Louai Labanieh at the University of California Irvine for the illustration.

■ REFERENCES

(1) Hertzberg, R. P.; Pope, A. J. *Curr. Opin. Chem. Biol.* **2000**, *4*, 445−451.
(2) Sundberg, S. A. *Curr. Opin. Biotechnol.* **2000**, *11*, 47−53.
(3) Hong, J.; Edel, J. B.; deMello, A. J. *Drug Discovery Today* **2009**, *14*, 134−146.
(4) Breslauer, D. N.; Lee, P. J.; Lee, L. P. *Mol. BioSyst.* **2006**, *2*, 97−112.
(5) Sackmann, E. K.; Fulton, A. L.; Beebe, D. J. *Nature* **2014**, *507*, 181−189.
(6) Whitesides, G. M. *Nature* **2006**, *442*, 368−373.
(7) DeMello, A. J. *Nature* **2006**, *442*, 394−402.
(8) Elvira, K. S.; Casadevall i Solvas, X.; Wootton, R. C.; deMello, A. J. *Nat. Chem.* **2013**, *5*, 905−915.
(9) Tomazelli Coltro, W. K.; Cheng, C. M.; Carrilho, E.; de Jesus, D. P. *Electrophoresis* **2014**, *35*, 2309−2324.
(10) Song, H.; Tice, J. D.; Ismagilov, R. F. *Angew. Chem., Int. Ed.* **2003**, *42*, 768−772.
(11) Teh, S. Y.; Lin, R.; Hung, L. H.; Lee, A. P. *Lab Chip* **2008**, *8*, 198−220.
(12) Gunther, A.; Jensen, K. F. *Lab Chip* **2006**, *6*, 1487−1503.
(13) Kang, D. K.; Ali, M. M.; Zhang, K. X.; Huang, S. S.; Peterson, E.; Digman, M. A.; Gratton, E.; Zhao, W. A. *Nat. Commun.* **2014**, *5*, 5427.
(14) Kang, D. K.; Ali, M. M.; Zhang, K. X.; Pone, E. J.; Zhao, W. A. *TrAC, Trends Anal. Chem.* **2014**, *58*, 145−153.
(15) Clausell-Tormos, J.; Lieber, D.; Baret, J. C.; El-Harrak, A.; Miller, O. J.; Frenz, L.; Blouwolff, J.; Humphry, K. J.; Koster, S.; Duan, H.; Holtze, C.; Weitz, D. A.; Griffiths, A. D.; Merten, C. A. *Chem. Biol.* **2008**, *15*, 427−437.
(16) Miller, O. J.; El Harrak, A.; Mangeat, T.; Baret, J. C.; Frenz, L.; El Debs, B.; Mayot, E.; Samuels, M. L.; Rooney, E. K.; Dieu, P.; Galvan, M.; Link, D. R.; Griffiths, A. D. *Proc. Natl. Acad. Sci. U. S. A.* **2012**, *109*, 378−383.
(17) Tran, T. M.; Lan, F.; Thompson, C. S.; Abate, A. R. *J. Phys. D: Appl. Phys.* **2013**, *46*, 114004.
(18) He, M.; Edgar, J. S.; Jeffries, G. D.; Lorenz, R. M.; Shelby, J. P.; Chiu, D. T. *Anal. Chem.* **2005**, *77*, 1539−1544.
(19) Benz, C.; Retzbach, H.; Nagl, S.; Belder, D. *Lab Chip* **2013**, *13*, 2808−2814.
(20) Srisa-Art, M.; Kang, D. K.; Hong, J.; Park, H.; Leatherbarrow, R. J.; Edel, J. B.; Chang, S. I.; deMello, A. J. *ChemBioChem* **2009**, *10*, 1605−1611.
(21) Choi, J. W.; Kang, D. K.; Park, H.; deMello, A. J.; Chang, S. I. *Anal. Chem.* **2012**, *84*, 3849−3854.
(22) Srisa-Art, M.; deMello, A. J.; Edel, J. B. *Chem. Commun.* **2009**, 6548−6550.
(23) Dressler, O. J.; Maceiczyk, R. M.; Chang, S. I.; deMello, A. J. *J. Biomol. Screening* **2014**, *19*, 483−496.
(24) Niu, X.; Gielen, F.; Edel, J. B.; deMello, A. J. *Nat. Chem.* **2011**, *3*, 437−442.
(25) Song, H.; Ismagilov, R. F. *J. Am. Chem. Soc.* **2003**, *125*, 14613−14619.
(26) Gielen, F.; Buryska, T.; Van Vliet, L.; Butz, M.; Damborsky, J.; Prokop, Z.; Hollfelder, F. *Anal. Chem.* **2015**, *87*, 624−632.
(27) Lim, J.; Caen, O.; Vrignon, J.; Konrad, M.; Taly, V.; Baret, J. C. *Biomicrofluidics* **2015**, *9*, 034101.
(28) Damean, N.; Olguin, L. F.; Hollfelder, F.; Abell, C.; Huck, W. T. *Lab Chip* **2009**, *9*, 1707−1713.
(29) Ho, C. M.; Ng, S. H.; Li, K. H.; Yoon, Y. J. *Lab Chip* **2015**, *15*, 3627−3637.
(30) Eastburn, D. J.; Sciambi, A.; Abate, A. R. *Anal. Chem.* **2013**, *85*, 8016−8021.
(31) Mazutis, L.; Gilbert, J.; Ung, W. L.; Weitz, D. A.; Griffiths, A. D.; Heyman, J. A. *Nat. Protoc.* **2013**, *8*, 870−891.
(32) Cho, S.; Kang, D. K.; Sim, S.; Geier, F.; Kim, J. Y.; Niu, X. Z.; Edel, J. B.; Chang, S. I.; Wootton, R. C. R.; Elvira, K. S.; deMello, A. J. *Anal. Chem.* **2013**, *85*, 8866−8872.
(33) Jeon, N. L.; Dertinger, S. K. W.; Chiu, D. T.; Choi, I. S.; Stroock, A. D.; Whitesides, G. M. *Langmuir* **2000**, *16*, 8311−8316.
(34) Dertinger, S. K. W.; Chiu, D. T.; Jeon, N. L.; Whitesides, G. M. *Anal. Chem.* **2001**, *73*, 1240−1246.
(35) Walker, G. M.; Monteiro-Riviere, N.; Rouse, J.; O'Neill, A. T. *Lab Chip* **2007**, *7*, 226−232.
(36) Wegrzyn, J.; Samborski, A.; Reissig, L.; Korczyk, P. M.; Blonski, S.; Garstecki, P. *Microfluid. Nanofluid.* **2013**, *14*, 235−245.
(37) Huebner, A.; Srisa-Art, M.; Holt, D.; Abell, C.; Hollfelder, F.; Demello, A. J.; Edel, J. B. *Chem. Commun.* **2007**, 1218−1220.
(38) Stefanini, M. *Cancer* **1985**, *55*, 1931−1936.
(39) Ahrens, M. J.; Bertin, P. A.; Vonesh, E. F.; Meade, T. J.; Catalona, W. J.; Georganopoulou, D. *Prostate* **2013**, *73*, 1731−1737.
(40) Hadler-Olsen, E.; Winberg, J. O.; Uhlin-Hansen, L. *Tumor Biol.* **2013**, *34*, 2041−2051.
(41) Zhang, J. M.; Yang, P. L.; Gray, N. S. *Nat. Rev. Cancer* **2009**, *9*, 28−39.
(42) D'Amelio, M.; Cavallucci, V.; Middei, S.; Marchetti, C.; Pacioni, S.; Ferri, A.; Diamantini, A.; De Zio, D.; Carrara, P.; Battistini, L.; Moreno, S.; Bacci, A.; Ammassari-Teule, M.; Marie, H.; Cecconi, F. *Nat. Neurosci.* **2011**, *14*, 69−76.
(43) Chhanabhai, M.; Krajewski, S.; Krajewska, M.; Wang, H. G.; Reed, J. C.; Gascoyne, R. D. *Blood* **1997**, *90*, 2451−2455.
(44) Izban, K. F.; Wrone-Smith, T.; Hsi, E. D.; Schnitzer, B.; Quevedo, M. E.; Alkan, S. *Am. J. Pathol.* **1999**, *154*, 1439−1447.
(45) Yamada, M.; Kida, K.; Amutuhaire, W.; Ichinose, F.; Kaneki, M. *Biochem. Biophys. Res. Commun.* **2010**, *402*, 312−318.
(46) Thompson, C. B. *Science* **1995**, *267*, 1456−1462.
(47) Hanahan, D.; Weinberg, R. A. *Cell* **2000**, *100*, 57−70.
(48) Yuan, J.; Yankner, B. A. *Nature* **2000**, *407*, 802−809.
(49) Green, D. R.; Evan, G. I. *Cancer Cell* **2002**, *1*, 19−30.
(50) Vaux, D. L.; Flavell, R. A. *Curr. Opin. Immunol.* **2000**, *12*, 719−724.
(51) Porter, A. G.; Janicke, R. U. *Cell Death Differ.* **1999**, *6*, 99−104.
(52) Hug, H.; Los, M.; Hirt, W.; Debatin, K. M. *Biochemistry* **1999**, *38*, 13906−13911.
(53) Liu, J. X.; Bhalgat, M.; Zhang, C. L.; Diwu, Z. J.; Hoyland, B.; Klaubert, D. H. *Bioorg. Med. Chem. Lett.* **1999**, *9*, 3231−3236.
(54) Yoshimori, A.; Takasawa, R.; Tanuma, S. *BMC Pharmacol.* **2004**, *4*, 7.
(55) Feng, Y.; Mitchison, T. J.; Bender, A.; Young, D. W.; Tallarico, J. A. *Nat. Rev. Drug Discovery* **2009**, *8*, 567−578.
(56) Kim, J. Y.; Baek, J. Y.; Lee, K. A.; Lee, S. H. *Sens. Actuators, A* **2005**, *119*, 593−598.
(57) Mogi, K.; Fujii, T. *Lab Chip* **2013**, *13*, 1044−1047.
(58) Bhargava, K. C.; Thompson, B.; Malmstadt, N. *Proc. Natl. Acad. Sci. U. S. A.* **2014**, *111*, 15013−15018.
(59) McDonald, J. C.; Whitesides, G. M. *Acc. Chem. Res.* **2002**, *35*, 491−499.

DOI: 10.1021/acs.analchem.5b02402
Anal. Chem. 2015, 87, 10770−10778

(60) Chen, C. H.; Sarkar, A.; Song, Y. A.; Miller, M. A.; Kim, S. J.; Griffith, L. G.; Lauffenburger, D. A.; Han, J. *J. Am. Chem. Soc.* **2011**, *133*, 10368−10371.
(61) Edel, J. B.; Hill, E. K.; de Mello, A. J. *Analyst* **2001**, *126*, 1953−1957.
(62) Stavis, S. M.; Edel, J. B.; Li, Y. G.; Samiee, K. T.; Luo, D.; Craighead, H. G. *Nanotechnology* **2005**, *16*, S314−S323.

DOI: 10.1021/acs.analchem.5b02402
Anal. Chem. 2015, 87, 10770−10778